Biosensors and Bioelectronics 296 (2026) 118295

Contents lists available at ScienceDirect

Biosensors and Bioelectronics

journal homepage: www.elsevier.com/locate/bios

FFF as a microfluidic platform for the streamlined optimization of ready-to-use nanozyme-labelled probes to enable robust and ultra-sensitive chemiluminescent bioassays

Luisa Stella Dolci [a,1], Valentina Marassi [b,c,d,1], Stefano Giordani [b,c,d], Deborah Pedone [f], Anna Placci [b,c,d], Virginia Rondinini [b], Erika Scavetta [a], Pierluigi Reschiglian [b,c,d], Mauro Moglianetti [e,f], Pier Paolo Pompa [f,g], Andrea Zattoni [b,c,d,*], Barbara Roda [b,c,d,**], Aldo Roda [b,c]

[a] Department of Industrial Chemistry "Toso Montanari", University of Bologna, Via Piero Gobetti 85, Bologna, Italy
[b] Department of Chemistry G. Ciamician, University of Bologna, Italy
[c] byFlow srl, Bologna, Italy
[d] INBB, National Institute of Biostructure and Biosystems, Rome, Italy
[e] Center for Cultural Heritage Technology CCHT, Istituto Italiano di Tecnologia (IIT), Via Torino 155, Venezia Mestre, 30172, Italy
[f] Nanobiointeractions & Nanodiagnostics, Istituto Italiano di Tecnologia (IIT), Via Morego 30, 16163, Genova, Italy
[g] College of Optical Science and Engineering, Zhejiang University, Hangzhou, 310058, China

ARTICLE INFO

Keywords:
Ultrasmall Pt nanoenzymes
Hollow-fiber flow field-flow fractionation
Isolation of conjugated ultrasmall
Chemiluminescent biosensors
Quality control of nanoenzymes

ABSTRACT

The replacement of enzyme labels such as horseradish peroxidase (HRP) with noble metal nanoparticles represents a promising approach in biosensing. Ultrasmall platinum nanoparticles (PtNPs) exhibit remarkable catalytic activity, chemical stability, and low production costs, making them attractive nanozyme candidates also in the field of highly sensitive chemiluminescence (CL) detection. However, their CL performances strongly depend on particle size, shape, composition, and concentration, often resulting in limited reproducibility and robustness. These physicochemical parameters also affect biomolecular labeling efficiency, including conjugation with proteins and antibodies, which is critical for consistent biosensor performance. To enable the development of robust biosensors integrating nanozymes as active sensing elements, rigorous nanoparticle quality control and efficient isolation of their bioconjugates are key steps. In this work, we report the first application of hollow-fiber flow field-flow fractionation (HF5) for the characterization and isolation of bioconjugated ultrasmall PtNPs designed for CL bioassays. Shape-controlled pyramidal PtNPs were synthesized in aqueous media via a rapid, scalable, and surfactant-free route exploiting sodium citrate as a shape-directing agent. PtNPs were characterized to define optimal nanoparticle-to-protein ratios, ensuring high conjugate stability. HF5 was then employed to selectively isolate standardized conjugated PtNPs, which were directly employed for CL signal generation. Finally, a proof-of-concept study demonstrated the use of conjugated IgG-PtNPs isolated through HF5 for the quantitative detection of a primary antibody in a paper-based CL bioassay, achieving a limit of detection suitable for diagnostic applications. Thus, HF5-mediated streamlining of probe synthesis and isolation offered a very promising answer to unmet needs in biosensor development.

1. Introduction

In the latest years, impressive advances in biosensing and clinical diagnostics have taken place due to the development of new *nanomaterials with intrinsic enzyme-like* properties called "nanozymes" (Wei and Wang, 2013; Calabria et al., 2021). Notably, nanomaterial-based artificial enzymes, namely nanoparticles endorsed with catalytic properties and enzyme-like activities, represent a valid

* Corresponding author. Department of Chemistry G. Ciamician, University of Bologna, Italy.
** Corresponding author. Department of Chemistry G. Ciamician, University of Bologna, Italy.
E-mail addresses: andrea.zattoni@unibo.it (A. Zattoni), barbara.roda@unibo.it (B. Roda).
[1] Contributed equally.

https://doi.org/10.1016/j.bios.2025.118295
Received 31 July 2025; Received in revised form 14 November 2025; Accepted 3 December 2025
Available online 4 December 2025

alternative to the fragile and expensive proteins as a result of their long-term stability and versatility (Wei and Wang, 2013). At present, nanozymes can be considered some of the most promising options for biomedical and biotechnological fields (Wang et al., 2024), with a broad range of applications in biosensing/bioimaging from in vitro detection to immunodiagnostic in living systems. Nanozymes have been extensively integrated into biosensing platforms for the detection of a broad range of analytes, including small molecules (e.g., glucose, neurotransmitters), metal ions (e.g., mercury, lead), proteins, and whole cells for applications domains such as environmental monitoring, food safety, and clinical diagnostics. Recent progress in nanozyme-based sensor technologies has notably enhanced the detection capabilities for foodborne pathogens, pesticides, and other hazardous contaminants (Hamed et al., 2025). The rise of precision medicine has underscored the critical importance of early and accurate biomarker detection for disease diagnosis, staging, treatment planning, and prognosis. However, the low abundance of biomarkers in the early stages of disease presents significant challenges for traditional detection methodologies. In this context, nanozyme-based biosensors have emerged as promising alternatives due to their high sensitivity, ease of operation, and cost-effectiveness. Nanozyme-based wearable biosensors are also gaining significant traction in healthcare applications. These devices combine the advantages of nanozyme catalysis with the portability, cost-efficiency, and environmental adaptability of wearable formats, providing a powerful toolkit for real-time health monitoring and personalized medicine (Zhang et al., 2025a).

Platinum nanoparticles (PtNPs) have emerged as efficient enzyme substitutes, showing superior catalytic performances, strong robustness against harsh pH and temperature conditions, and easy and low-cost production with respect to Ag and Au NPs (Gatto et al., 2017; Pedone et al., 2017; Mirra et al., 2025; Cursi et al., 2024; Cupini et al., 2023; Bardi et al., 2023; Tarricone et al., 2023). Recent results highlight how the diagnostic field could strongly benefit from the ability of PtNPs to mimic horseradish peroxidase (HRP), one of the most widely used enzymes in biosensing (Scarsi et al., 2023). PtNPs are able to replace HRP in catalyzing the redox reaction between its chromogenic (e.g. 3,3′,5,5′-tetramethylbenzidine, TMB and 3,3′-diaminobenzidine, DAB) and chemiluminescent (CL) (e.g. luminol) substrates and the oxidizing agent hydrogen peroxide (H_2O_2) (Gatto et al., 2017). As an interesting feature, recent studies revealed that the large surface-active area of PtNPs could favor their strong affinity for these substrates (approximately 10 times higher than that of HRP) (DNA-Based Platinum Nanozymes for Peroxidase), ensuring high selectivity of the reaction. Since the first example of a PtNPs-based colorimetric immunoassay reported in the literature more than 10 years ago, several colorimetric biosensors employing them as detection probes have been developed for detecting cancer cells, metal ions, bacteria, and antioxidants (Gatto et al., 2017; Il Kim et al., 2014; Tseng et al., 2012; Pedone et al., 2020; Su et al., 2013). Furthermore, PtNPs have shown to be an ideal platform for the development of lateral flow immunoassays (LFIA) with enhanced sensitivity and stability (Calabria et al., 2021; Loynachan et al., 2018; Gao et al., 2017; Wei et al., 2020; Jiang et al., 2016; Wang et al., 2020a; Cheng et al., 2017; Liu et al., 2020; Gold-Platinum Nanoflowers as a Label). Loynachan et *al.* presented an ultrasensitive screening tool for the detection of p24 serum protein as HIV biomarker, exploiting a highly innovative detection scheme based on biotin−streptavidin binding and the oxidation of DAB substrate catalyzed by PtNPs (Loynachan et al., 2018). Exploiting a similar detection scheme, Jiang et *al.* proposed an ultrasensitive LFIA for the rapid (less than 1 min), quantitative, and simple detection of *E. coli* O157:H7 in foods (Jiang et al., 2016).

The catalytic activity of PtNPs can be tailored by modulating their size and shape, an advantage that combined with the use of synthesis methods avoiding the use of capping agents—thus leaving the surface suitable for the immobilization of recognition elements—makes these nanoparticles particularly attractive for biosensor development. Reduced dimensions together with specific surface structures were demonstrated to be able to improve catalytic properties, including kinetics and stability. Indeed, ultrasmall pyramidal PtNPs were successfully employed for cellular imaging via electron microscopy, leveraging their peroxidase-like activity to generate electron-dense signals for high-resolution tracking of biomolecules in complex intracellular environment (De Luca et al., 2024; Ruditskiy and Xia, 2017; Mastronardi et al., 2020; Hornberger et al., 2021).

In the field of diagnostic and biotechnological applications, CL and Bioluminescence (BL) are well-established detection techniques providing advantages in terms of sensitivity, rapidity, and suitability for miniaturization and biosensor formats, because of their very low nonspecific background signal and high signal-to-noise ratio (Reyes et al., 2022; Roda et al., 2020, 2024; Zhang et al., 2025b). More sophisticated CL reactions based on the use of Pt-bases nanocatalysts, in combination with luminol and H_2O_2, have also been exploited for the development of ultrasensitive biosensors for the detection of DNA, proteins, and tumor markers (Choi et al., 2017; Wang et al., 2020b; Xu and Cui, 2007). Interestingly, a 1000-fold higher sensitivity compared to traditional approaches for human chorionic gonadotropin detection has been achieved by exploiting the HRP-mimic properties of ultrasmall (2–3 nm) PtNPs in combination with a CL signal band, revealing the importance of the accurate control on the NP size for biosensing applications (Park et al., 2015).

Despite the promising applications of ultrasmall PtNPs in CL bioassays, only a few methods employing them have been developed so far. The analysis of published studies indicates that the CL catalytic activity of these ultrasmall nanoparticles—in terms of both signal intensity, kinetic profile and flash emission—is highly dependent on their size, shape, composition, and concentration (Xu and Cui, 2007) and lacks robustness. These physicochemical parameters critically influence both the catalytic activity per unit mass and the capacity for biomolecular labeling, including proteins and antibodies, employed when PtNPs have to be prepared as biosensing tool via various immobilization strategies. Among those for protein immobilization, physical methods offer several advantages in biosensing applications. Physisorption provides a straightforward and mild strategy for protein–nanoparticle conjugation since it minimizes the risk of protein denaturation or loss of biological activity often associated with more aggressive chemical coupling methods (Bhakta et al., 2015). Moreover, it enables conjugation under physiologically compatible conditions and frequently allows for better control over protein orientation while preserving functional integrity. It is to notice that nanoparticle curvature and surface geometry strongly influence adsorption dynamics by altering the spatial availability of binding sites. Nanoparticle size also affects the electrostatic double-layer potential, which in turn can influence protein conformation and adsorption behavior.

After conjugations process, the isolation of ultrasmall nanoparticles is commonly performed via chromatographic techniques and ultracentrifugation. Size exclusion chromatography (SEC) enables size-based separation of nanoparticles by utilizing a stationary phase composed of porous beads. A key challenge lies in the limited resolution for the separation of ultrasmall nanoparticles from the bioconjugation mixture, as well as non-specific interactions between nanoparticles and the stationary phase, which may compromise their native physicochemical properties. Ultrafiltration, employing membranes with well-defined molecular weight cut-offs, is often considered a more scalable and efficient method for isolating nanoparticle–biomolecule conjugates. Ultracentrifugation, although widely used for nanoparticle separation, presents several drawbacks when applied to small, conjugated nanoparticles. It is generally time-consuming, may require large sample volumes, and often lacks sufficient resolution to distinguish nanoparticles with subtle differences in size, density, or surface composition. Moreover, excessive centrifugal forces, prolonged centrifugation times, or suboptimal experimental conditions may lead to undesirable effects such as NP aggregation or non-specific protein sedimentation (Soliman et al., 2024). All these techniques exhibit low throughput and require

extensive sample manipulation, which limits their scalability for CL biosensing applications. Consequently, a precise production of well-defined conjugated NPs represents a fundamental step to control their catalytic activity and biofunctionalization: several analytical challenges remain in translating nanozyme-based biosensors from proof-of-concept studies to widespread practical use.

To fill this analytical gap, a field-flow fractionation (FFF)-multi-detection platform based on simultaneous signal detection using UV/vis DAD, fluorescence (FLD), multi-angle-light scattering (MALS) offers a suitable solution. FFF is a gentle, stationary phase-free separation technique that operates based on a laminar flow that transports analytes through a capillary channel and on the application of a perpendicular force generated through the channel's porosity (crossflow). FFF effectively separates NPs based on their diffusion coefficients or hydrodynamic sizes ranging from approximately 1 nm to several tens of micrometers, and even up to 100 μm (Lespes and De Carsalade Du Pont, 2022; Contado, 2017; Giordani et al., 2023); due to the soft separation mechanism the analytes native properties (morphology, activity, functional properties,..) are preserved during fractionation (Carvalho et al., 2018). Several applications were developed spanning from drug delivery, biomedical and bioassay applications, environmental monitoring and food quality assessment (Ramm et al., 2022; Sitar et al., 2017; Bian et al., 2023; López-Sanz et al., 2019; Sánchez-Cachero et al., 2021). In the area of bioassay development, Menéndez-Miranda et al. demonstrated how FFF-ICP-MS can be used to accurately quantify the efficiency of bioconjugation between quantum dots and antibodies (Ferreira et al., 2020).

In this work we present for the first time the use of the miniaturized version of FFF—hollow-fiber flow field-flow fractionation (HF5) as a powerful and versatile microfluidic platform for the characterization, optimization and isolation of bioconjugate ultrasmall PtNPs for CL bioassays (Tan et al., 2015, 2017; Marassi et al., 2019, 2025). Ultrasmall pyramidal platinum nanoparticles with a designed shape were synthesized in an aqueous medium using a rapid and easily scalable method, which exploits the shape-directing properties of sodium citrate molecules, without the need for hard-to-remove capping agents. The optimal conditions in terms of PtNPs:protein ratio were established, and the CL response of standardized conjugated PtNPs was thoroughly evaluated. Finally, a pilot study was described for the use of IgG-coated PtNPs, isolated through the HF5 for the CL quantification of a primary antibody in a paper-based analytical format, proving the translational potential of the HF5 approach to effectively streamline real-case probe production enabling prompt and robust development of CL biosensing formats.

2. Material and methods

2.1. Materials

Chloroplatinic acid hexahydrate (BioXtra specification), L-ascorbic acid (BioXtra specification, ≥99 %), sodium citrate tribasic dihydrate (BioUltra specification, ≥99 %), sodium borohydride (≥98 %), citric acid anhydrous (≥99 %), Bovine serum albumin (BSA) > 99 %, Na_2HPO_4•12 H2O > 99 %, $C_6H_6O_7Na_2$> 99 %, NaOH >98 %, peroxidase from horseradish Type VI-A, were bought from Sigma-Aldrich. NaCl >99 % was purchased from Fluka. KCl >99 %, HCl 37 %, Carlo Erba were bought from Carlo Erba. Goat anti-Rabbit IgG (H + L) Antibody and Rabbit anti-Mouse IgG (H + L) Antibody were purchased by Invitrogen. Nitrocellulose membrane Amersham® Protran® was bought from Sigma-Aldrich.

Phosphate buffered saline (PBS) was prepared as follows: 10 mmol L^{-1} Na_2HPO_4, 2 mmol L^{-1} KH_2PO_4, 137 mmol L^{-1} NaCl, 2.7 mmol L^{-1} KCl, pH 7.4.

For CL measurement, black 96-multiwell plate (Thermo Fisher Scientific) and the CL substrate Super Signal ELISA Femto (Thermo Fisher Scientific) were employed.

2.2. Synthesis and characterization of 4 nm pyramidal Pt nanoparticles

Pyramidal platinum nanoparticles (PtNPs) with an average size of 4 nm were synthesized following a previously established protocol (Mastronardi et al., 2022). Specifically, 150 μL of a 0.5 M hexachloroplatinic acid solution was introduced into 90 mL of Milli-Q water preheated to 90 °C under continuous magnetic stirring. After 1 min, 192 μL of a 0.5 M sodium citrate solution was added, followed by the dropwise addition of 5.7 mL of a freshly prepared 0.075 M sodium borohydride solution. The reaction vessel was immediately sealed and maintained at 90 °C for 10 min, after which the solution was allowed to cool to room temperature. The resulting nanoparticles were thoroughly purified using 30K Amicon Ultra Centrifugal Filters with a 2 mM sodium citrate solution and stored at 4 °C for subsequent analyses. The morphology and size distribution of the nanoparticles were characterized through bright-field transmission electron microscopy (BF-TEM).

2.3. PtNPs conjugation procedure

The bioconjugation of the PtNPs was performed through physisorption approach. BSA was primarily used in this work as a model protein to enable a cost-effective study, aimed at demonstrating the feasibility of using HF5 to optimize protein-based PtNPs catalytic conjugates for integration into CL assays. A series of mixtures (Table 1) with increasing PtNPs:BSA m/m ratio were prepared. The appropriate amount of the BSA was added to 1 mL of PtNPs in borate buffer (20 mM, pH 8) and incubated under gently stirring for 30 min at 37 °C.

The same procedure was also applied to prepare a mixture with PtNPs:anti-Rabbit IgG 1:1 (m/m) ratio.

2.4. HF5 platform for conjugated-PtNPs CL assay

2.4.1. HF5 analysis

HF5 analyses were performed using an Agilent 1200 HPLC system (Agilent Technologies, Santa Clara, CA, USA) combined with an Eclipse® DUALTEC separation system (Wyatt Technology Europe, Dernbach, Germany). The fiber was a type FUS 0181 polyethersulfone (PES) fiber, available from Microdyn-Nadir (Wiesbaden, Germany) with the following characteristics: 0.8 mm inner diameter, 1.3 mm outer diameter, and 10 kDa Mw cut-off. Online detection of the eluted species was performed with a series of detectors here reported based on their order of coupling: an Agilent 1100 DAD UV/Vis spectrophotometer, an Agilent 1200 spectrofluorometer and a MALS detector operating at 658 nm wavelength model DAWN HELEOS (Wyatt Technology Corporation, Santa Barbara, CA, USA). The spectrofluorometer was set to work using a 280 nm absorption wavelength and a 340 nm emission wavelength to selectively monitor BSA. Data collection was performed by the software ChemStation version B.04.02 and ASTRA® software version 6.1.7 (Wyatt Technology Corporation, Santa Barbara, CA, USA).

The developed method exploited a constant detector flow set at 0.35 mL/min, while the focus step, which lasted 3 min, was characterized by a 0.8 mL/min focus flow. During the elution step of the separation method, the crossflow was kept constant at 0.8 mL/min for 10 min then

Table 1
List of samples prepared to monitor the conjugation rate as a function of the ratio between PtNPs and BSA.

Sample	Pt: BSA (m/m)
BSA	/
MIX A	0.2 : 1
MIX B	0.4 : 1
MIX C	0.6 : 1
MIX D	1 : 1
MIX E	1.4 : 1
MIX F	2 : 1

decayed exponentially from 0.8 mL/min to 0 mL/min over 3 min (Slope = 3) and remained then constant for 8min.

According to FFF theory, retention time is inversely proportional to the hydrodynamic diffusion coefficient of the analyte and, consequently, to its molecular weight (Mr) or hydrodynamic radius (Rh), as described by the Stokes equation. The hydrodynamic radii were determined based on FFF theory using the ISIS software (Wyatt Technology Europe) for method size calibration (Dubascoux et al., 2008).

Isotonic PBS pH 7.4 was used as mobile phase to obtain results representative of the real environment in which the nanozyme-protein device would be used while implemented in a biosensor.

Repeatability, reproducibility and membrane performances were assessed both on retention times and on signal intensity by performing three independent replicates (both intra- and inter-day) for BSA solution. Recovery was calculated as the percentage ratio between the integrated area obtained from the separative method described above and a Flow Injection Analysis respectively (Marassi et al., 2023; Zappi et al., 2022). The latter is a non-separative analysis characterized by the absence of a focusing step and a separative force. Here, the sample is carried quantitatively to the detector and the signal is associated to the whole sample content.

2.4.2. CL measurement

The SuperSignal ELISA Femto CL substrate was prepared by mixing reagent A and B immediately before the sample addition. This CL cocktail contains the luminol, H_2O_2 and two enhancers which strongly improve the CL signal intensity forming a steady state. A volume of 20 μL of sample solutions was added in a black 96-well plate, then acquisition is performed after the addition of 180 μL of the CL substrate. The CL signal was acquired with a Varioskan™ LUX multimode microplate reader (Thermofisher) for 30 min with an integration time of 200 ms; and it was expressed as relative light unit (RLU). All the experiments were carried out in triplicate.

2.5. Dot-immunobinding assay

A non-competitive sandwich-type immunoassay for the quantitative detection of IgG was developed as a pilot study to evaluate the use of isolated antibody-conjugated PtNPs in a biosensor system.

Solutions of Rabbit IgG at different concentrations (0,08 to 0,5 ng/mL) were spotted onto a nitrocellulose membrane using a calibrated microcapillary tube by depositing 1 μL solution in borate buffer (pH 8.5) and drying at RT for 10 min. The membrane was then incubated with 1 % BSA blocking solution for 1 h at RT. After three washes with PBS 0.1 M containing 0.1 % BSA, the membrane was incubated for 1 h at 37 °C with the PtNPs:(anti-Rabbit) IgG conjugate, previously isolated by HF5. The membrane was washed with PBS 0.1M to remove unbound conjugate from the sample and finally the CL substrate was added.

The CL signal was acquired using an high sensitive smartphone CMOS, A mini-dark box (2 × 1.5 × 1.5 cm) in acrylonitrile butadiene styrene containing the nitrocellulose strip was designed to fit a smartphone equipped with a high-performance (BSI)-CMOS (sensor size 1/2.5″, aperture size F1.7, resolution of 4290 × 2800 pixels) in acrylonitrile butadiene styrene (ABS). The CL substrate was added through a capillary. Digital images (90 s of acquisition) were analyzed employing ImageJ software v.1.46 (National Institutes of Health, Bethesda, MD). The intensity of the CL signal was measured in the area corresponding to the test spot and subtracted of the mean background signal measured in adjacent areas; values were used to generate a calibration curve.

3. Results and discussion

3.1. Synthesis and characterization of pyramidal platinum nanoparticles (PtNPs)

Citrate buffer-stabilized pyramidal PtNPs were synthesized following the methodology described by Mastronardi et al. (2022), employing a rapid, scalable, and straightforward aqueous-phase procedure that predominantly uses biogenic compounds. The reaction is performed with a simple setup. Sodium citrate is employed as a stabilizing agent to ensure colloidal stability in the aqueous phase. The subsequent dropwise addition of sodium borohydride enables a controlled reduction process, promoting the formation of pyramidal nanostructures through the breaking of symmetry driven by the selective adsorption of hydrogen on the growing nanocrystals (Nelli et al., 2023).

Morphological and structural characterization of the synthesized PtNPs was performed using bright-field transmission electron microscopy (BF-TEM) and High-angle annular dark-field scanning transmission electron microscopy (HAADF STEM). The nanoparticles exhibited a well-defined pyramidal morphology with an average edge length of 3.5 ± 0.7 nm (Supplementary materials, Fig. S1). High-resolution transmission electron microscopy (HR-TEM) provided detailed insights into the crystallographic features of the nanopyramids (Mastronardi et al., 2022), proving the presence of four dominant (111) facets and five truncated (100) facets at the particle corners, along with a single, more elongated (100) facet forming the base of the pyramid. Statistical analysis revealed that over 75 % of the particles displayed pyramidal morphology.

A theoretical structural model generated using VESTA (Mastronardi et al., 2022) for a nanoparticle with an edge length of 3.5 nm, demonstrated that approximately 50 % of the total atomic population resides on the nanoparticle surface. This high surface atom fraction enhances catalytic efficiency, maximizing the active sites available for reactions while reducing the quantity of precious metal required. The catalytic properties of metallic nanoparticles are intrinsically linked to their size and shape, which dictate the exposure of specific crystallographic facets (Mastronardi et al., 2022). The pyramidal PtNPs synthesized in this study are ideally suited to achieve enhanced catalytic performance compared to spherical counterparts, owing to their well-defined surface structures (Mazzotta et al., 2023).

3.2. HF5: characterization of PtNPs, BSA and conjugated-PtNPs

3.2.1. HF5 separation

The conjugation of nanozymes to recognition elements is a critical aspect with consequences in downstream applications. Even though citrate-coated PtNPs show good colloidal stability in water, they present stability issues in high ionic strength media, such as physiological and assaying conditions commonly employed in bioassays. Therefore, conjugation steps and conjugate isolation could lead to complex scenarios, hard to quantify, and often yield a mixture of free and bound particles which hinder reproducibility and, hence, practical application.

An HF5 method able to separate protein and PtNPs was developed. First, HF5 separation performances for BSA and PtNPs were studied. Equal amounts of BSA (200 ppm, PBS) and PtNPs (200 ppm of Pt, MilliQ) solutions were separately injected into the device to evaluate their elution time and recovery, as described in *Materials and Methods*. PtNPs and BSA (d_h monomer: 7 nm) have similar hydrodynamic sizes, making extremely challenging to elute them at different retention times. To potentially separate the two species as well as monitor the slightest changes in size due to their reciprocal interactions, we developed a method characterized by a high separative power for particles in the low-nanometer range, having a d_h below 30 nm (Fig. 1), calibrated as described in *Materials and Methods*. BSA and PtNPs were selectively monitored following the fluorescence signal (protein specific) and the absorbance signal at 250 nm at which the BSA contribution is negligible (Fig. 1, inset). The method allowed separation of BSA monomer (t_r: 9.4 min) from dimer (t_r: 11.2 min) and further aggregates (t_r > 12 min) and was characterized by excellent recovery (>90 %). PtNPs injections showed a flat signal (therefore 0 % recovery; not shown). This behaviour is common for naked metal nanoparticles in a high saline environment (used as mobile phase) and can be explained by the large precipitation of

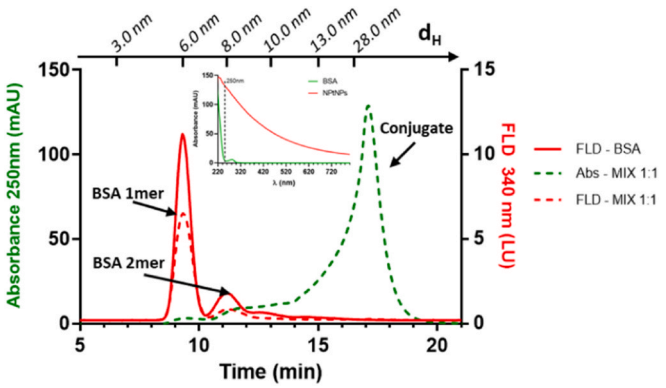

Fig. 1. UV (250 nm) and FLD fractograms of the injections of BSA alone and mix 1:1 (PtNPs: BSA). Red continuous trace: FLD signal of 5 μg of BSA. Red dotted trace: FLD signal of the injection of an equivalent mass of BSA incubated 1:1 with PtNPs. Green dotted trace: UV (250 nm) signal of the mix 1:1 (PtNPs: BSA) injection. Inset: UV/Vis spectrum of a 100 ppm solution of BSA (green trace), UV/Vis spectrum of a 100 ppm (Pt) solution of PtNPs (red trace). (For interpretation of the references to color in this figure legend, the reader is referred to the Web version of this article.)

the sample on the fiber during the focusing step due to the loss of electrostatic repulsion in high ionic strength media, resulting in the absence of an eluting peak.

Then, the HF5 method was applied to the analysis of the conjugated PtNPs. A 1:1 mixture of the starting 200 ppm BSA and PtNPs solution was prepared and injected (in triplicate) with the same final amount of PtNPs and BSA used in single injections. A typical fractographic profile is reported in Fig. 1. The UV signal (dashed green trace) highlighted the presence of a new broad and intense peak eluting between 9 and 20 min and peaking in intensity in the range between 14 and 18 min. The signal intensity, as well as the hydrodynamic size associated to the majority of the eluting band ($d_h > 10$ nm), suggest that the newly formed signal is associated to some PtNPs related species bigger than the original particles and stable in the channel. Further insight on the nature of the peak was provided by the specific BSA FLD-signal, which was lower than the one associated to the injection of same amount of BSA alone, indicating that part of the protein had interacted with the Pt particles. The absence of the FLD signal in correspondence to the conjugate peak can be explained by the quenching effect of PtNPs (Xu et al., 2024).

These observations suggest that (1) the protein act as a stabilizer of PtNPs; and (2) a portion of BSA interacts with the PtNPs generating the conjugated species ($PtNP_x$ - BSA_y) that elute after 12 min, enabling the reliable separation of a well-defined conjugated species from complex conjugation mixtures.

The intrinsic instability of bare PtNPs in PBS, and their subsequent stabilization upon conjugation with BSA, can be rationalized based on colloidal chemistry principles and nanoparticle–biomolecule surface interactions. In PBS, ionic species effectively screen the surface charges of PtNPs, reducing electrostatic repulsion, and thereby facilitating particle aggregation. Due to the absence of a stabilizing surface coating and a low amount of citrate, bare PtNPs are particularly susceptible to van der Waals attractions, which dominate interparticle interactions and promote agglomeration. Additionally, partial surface oxidation of PtNPs in aqueous environments may further alter their surface charge and exacerbate colloidal destabilization. In contrast, BSA acts as an effective stabilizing agent for PtNPs through multiple synergistic mechanisms. Upon adsorption, BSA introduces a steric barrier that physically hinders close particle–particle contact. At physiological pH, BSA possesses a net negative charge, enhancing electrostatic repulsion between conjugated nanoparticles. Specific amino acid residues—such as cysteine and lysine—facilitate direct binding to the PtNPs surface, thereby reducing surface energy and mitigating oxidative processes. Moreover, BSA conjugation increases the hydrophilicity of the nanoparticle surface, improving colloidal stability and dispersion in high-ionic-strength environments such as PBS.

3.2.2. *Investigation of the conjugating step*

To explore the use of HF5 to study the conjugation phenomenon and evaluate the stability and properties of the PtNPs-conjugates, a series of mixes (Table 1) with increasing PtNPs:BSA ratio were prepared and analyzed in HF5 with the developed method. The injection volume was adjusted to ensure that an equivalent amount of BSA protein (5 μg) was injected for each mixture. With the increase of PtNPs amount in the mix, a progressive decrease in the BSA-specific signal was observed, although free BSA remained in excess in the environment for all ratios (Fig. 2, I). The evolution of the 250 nm UV signal for the injection of conjugated PtNPs was characterized by an increase of signal from MIX A to MIX D, as noticeable by the rising band around 18 min. However, increasing the PtNPs:BSA mixing ratio beyond 1 (MIX E and F) did not lead to an increase in the signal associated with the complex but rather to its decrease (Fig. 2, II). These results suggest that a conjugation limit is reached, beyond which conjugate precipitation is observed as highlighted by the decrease of conjugate peak signal for mix E and F (Fig. 2, II), indicating a colloidal stability only for conjugates formed from mixtures A-D.

The amount of BSA conjugated to the platinum can be calculated by monitoring the decrease of the corresponding FLD signal, since the Pt quenching in the conjugated peak does not allow to monitor it otherwise (Xu et al., 2024). Assuming all the injected PtNPs, stabilized by BSA, is totally recovered from the channel (as verified in method development) and considering the drop in the BSA signal already discussed, we estimated the average conjugation ratio of the formed conjugate from triplicate analyses (Fig. 2, III), as well as its composition in terms of the concentration of the two species (Fig. 2, IV) for mixture A-D. Notably, a progressive rise in the PtNPs:BSA conjugation ratio is observed, suggesting a mechanism in which PtNPs progressively increases the conjugation rate with BSA. The analyses also show that this process continues until a limit is reached. The low standard deviation observed among three independent injections of identically prepared mixtures indicates the high reproducibility of the conjugation process.

From these results, it was possible to estimate a mean structure of the (PtNPs-BSA) complex in the mixtures A-D (Fig. 2, V). It was previously shown that the adsorption of BSA on platinum nanoparticles often results in multilayer structures (Yang et al., 2024). BSA is a multifunctional, and biocompatible biomacromolecule, that offers multiple binding sites for transition metal ions (Li et al., 2015). Owing to the chemical heterogeneity of protein structures, their interaction with nanoparticle surfaces typically involves multiple binding sites and mechanisms. On the other hand, the weak interaction between citrate molecules and the Pt surface facilitates their easy displacement. In addition, platinum exhibits a strong affinity for sulfur-containing functional groups on the external surface of BSA. Among the key parameters, solution pH plays a pivotal role by modulating the surface charge of both the protein and the nanoparticle, thereby affecting the magnitude of electrostatic attraction. Additional factors, including the protein's isoelectric point, nanoparticle size and surface properties, as well as the presence of an oxide layer, further contribute to defining the adsorption behavior and the structural characteristics of the resulting protein layer. BSA. Among the key parameters, solution pH plays a pivotal role by modulating the surface charge of both the protein and the nanoparticle, thereby affecting the magnitude of electrostatic attraction. Additional factors, including the protein's isoelectric point, nanoparticle size and surface properties, as well as the presence of an oxide layer, further contribute to defining the adsorption behavior and the structural characteristics of the resulting protein layer.

In this scenario, HF5 data supports the occurrence of multilayer structures for the conjugated species ($PtNP_x$–BSA_y), resulting from the BSA adsorption. Indeed, the structures reported in Fig. 2, V are

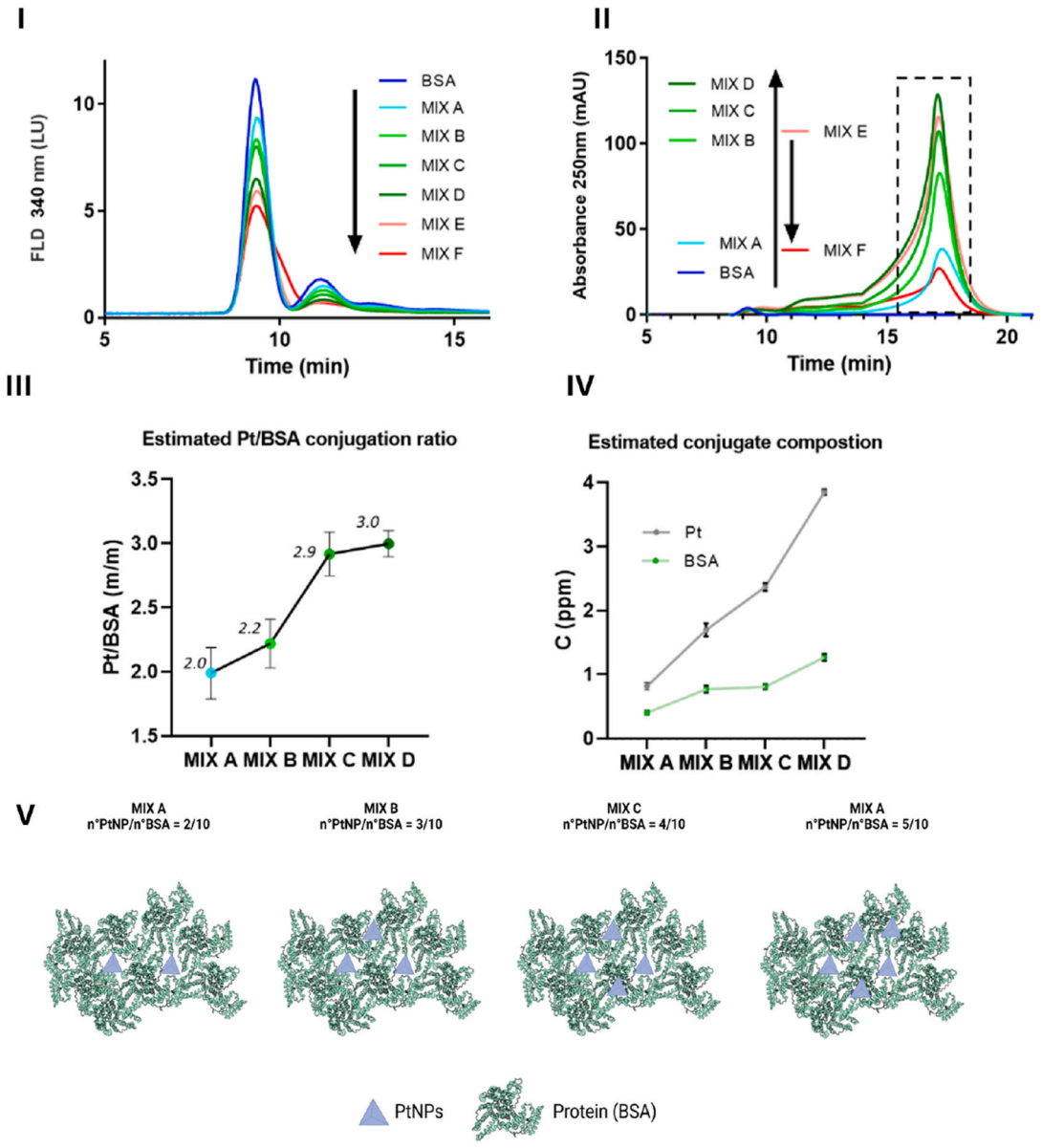

Fig. 2. Overview of the results of the injections of the samples described in Table 1. I. Representative FLD fractograms highlighting the decrease of the BSA free specific signal according to the increase of Pt concentration. II. Representative absorption fractograms (250 nm) highlighting the progressive increase of the conjugate complex according to the raising of Pt concentration. When the limit of stability is reached, significant sample precipitation is observed. The dotted box highlights the collection window. III. Average estimated conjugation ratio for the species in the collected fractions. IV. Average estimated concentration of Pt and BSA in the collected fractions. V. Estimated conjugate's structure (Created in https://BioRender.com).

compatible with dimensions determined by retention time as highlighted in Fig. 1, providing insights about (PtNPs-BSA) complexes and colloidal stability of PtNPs after bioconjugation.

To assess the stability of the conjugates over storage time, aliquots of the same mixtures were analyzed by HF5 24 and 72 h after their initial preparation (data not shown). The resulting elution profiles were found to be superimposable with those obtained immediately after preparation, confirming the structural stability and integrity of the conjugates over time in PBS buffer, without the need for stabilizing agents typically required when proteins are employed as biosensing elements. This result is particularly relevant and supports the potential implementation of these systems as nanozymes integrated into portable and robust diagnostic platforms.

3.3. CL performances of the conjugate-PtNPs

Given the ability of PtNPs to catalyse the CL oxidation of luminol, we quantified the performance of the selected and HF5-isolated PtNPs-protein conjugates.

3.3.1. CL activity of isolated BSA-PtNPs

The conjugated-PtNPs peak was collected for mixtures A-D at the end of the separation system (collection window: 15.5–18.5 min, Fig. 2II) and directly used for CL measurements. The BSA injection was also collected according to the same collection window and used as control of the CL experiments. The CL substrate was added (as previously described in *Materials and Methods section)* immediately after collection, and the kinetic emission was characterized with a benchtop luminometer.

In Fig. 3I the typical CL response curves are reported. PtNPs greatly

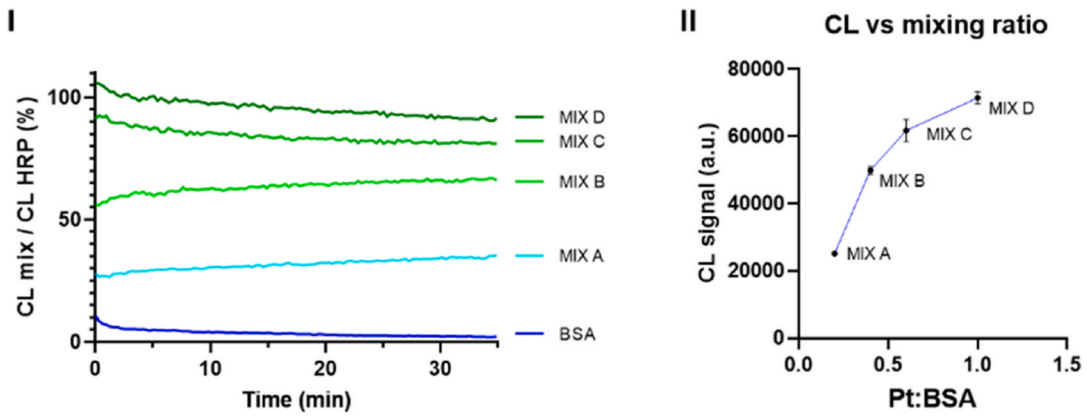

Fig. 3. I. Average CL signals over time of the collected fraction for each mix. **II.** CL signals (25min) of the collected fractions plotted against their corresponding Pt:BSA mixing ratio (Table 1).

enhance luminol–H_2O_2 CL, while no significant enhancement effect was found for the BSA-obtained fraction. The in-depth exploration of the catalytic mechanism of these nanoparticles is beyond the scope of this work; however, the luminophore of the CL system can be identified as the excited-state 3-aminophthalate anions (3-AP2−*). The catalytic effect of PtNPs is able to accelerate the electron-transfer process and facilitate the CL radical generation taking place on the surface of platinum nanoparticles in aqueous solution (Xu and Cui, 2007).

As reported in Fig. 3I, the CL signal reaches a plateau of steady state emission in less than 15 min and then remains constant for over 15 min, offering a plateau time window useful for analytical measurements. The enhancement effect is also dependent on conjugation ratio. For reference, the CL kinetics of HRP—one of the most commonly used enzyme labels in biosensors due to its low limit of detection (LOD) and broad linear range—was measured under identical CL substrate conditions. Data are normalized to the CL kinetic of an HRP solution at a concentration of 10 ng/mL, usually able to generate a high intense signal and commonly used in methods characterized by low LOD. Among different conjugates, mixture D shows the highest efficiency for CL catalytic activity. Data reported in Fig. 3I highlight that the CL catalytic activity of the homogeneous conjugated-PtNPs obtained through HF5 is comparable to that of a HRP solution measured in optimal substrate conditions, i.e. using a luminol-based CL substrate and enhancer already established for the enzyme to stabilize and amplify the CL signal.

Hence, the CL signal was measured at t = 25 min for each mixture to assess the emission efficiency. Averaged results for the three independent HF5-isolated replicates for each mixture are reported in Fig. 3II. The CL signal increases with the mixing ratio up to MIX D, following a trend that approaches to a plateau as the conjugates reach their stability limit. The values also show high reproducibility for each mixture. The conjugate from MIX D, which contain the highest PtNPs concentration (before the stability trend reversed), exhibit the strongest CL signal. This finding proves that a 1:1 (m/m) Pt:BSA ratio is the optimal combination for achieving the best CL active fraction.

We further evaluated the catalytic efficacy of the conjugated-PtNPs isolated for Mix D. The analytical performance of this catalytic system was assessed by constructing a calibration curve over a PtNPs concentration range of 0.04–4 μg/mL (Supplementary materials, Fig. S2). The calibration curve demonstrated a strong linear correlation ($R^2 > 0.99$) between the CL signal to blank ratio and the amount of conjugated-PtNPs across the entire range. The observed CL signal to blank ratios were comparable to those reported for various immuno- and biosensor formats utilizing HRP as the catalytic component (Roda et al., 2020). Notably, the calibration curve exhibits linearity over at least two orders of magnitude, highlighting the potential and demonstrating the suitability of the conjugated PtNPs as a catalyst for the development of various CL-based assay formats. The LOD, calculated as the mean blank value plus three times the standard deviation, was determined to be 0.005 μg/mL, corresponding to 0.001 μg of PtNPs-based catalyst per well. This LOD is notably lower than the catalytic amounts typically required in conventional NPs-based immunosensor systems (Park et al., 2015).

To further characterize the conjugated PtNPs noenzymes isolated through HF5 as potential sensing tool in robust biosensors, luminescence tests were conducted on the collected fraction (1:1) stored at both 4 °C for 24, 72 and 168 h; and room temperature (25 °C) for 24 and 72 h in PBS. The CL signal at t = 25 min for each condition was reported in Fig. 4. All samples showed no significant differences compared to MIX D analyzed immediately after preparation, regardless of the storage conditions, highlighting the remarkable stability of the catalytic activity even under simple RT storage, and the stability of the isolated conjugate in PBS.

These data together with the structural stability discussed in paragraph 3.2.2. Demonstrate that HF5 not only provides a well-defined nanoparticle–protein conjugate and enables standardization of the protein-to-nanoparticle ratio but also is able to isolate robust systems that can be used directly for sensitive CL-based sensing or stored for later use. Further investigations on the stability of conjugates can be focused on different conditions based on the specific recognition element used

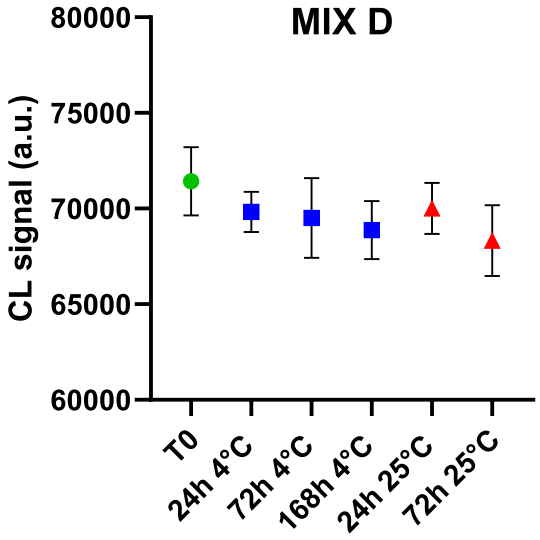

Fig. 4. Average CL signal (25min) of the MIX D fraction immediately after collection. and stored at both 4 °C for 24, 72 and 168 h; and room temperature (25 °C) for 24 and 72 h. No statistical differences are observed between averages (*t*-test).

and application.

3.3.2. HF5-mediated CL dot-immunobinding assay

To investigate the applicability of conjugated PtNPs in a CL biosensor, we devised a pilot study where a conventional sandwich-type immunosensor was developed for IgG determination, employing a nitrocellulose membrane as the solid-phase support for the diagnostic immunoassay. Indeed, since IgG represents the principal antibody involved in the adaptive immune response, its detection provides a well-established analytical approach for assessing infection.

A 1:1 (m/m) (anti-Rabbit IgG:PtNPs mixture was prepared, based on the knowledge acquired in the model study with BSA and aiming at producing the conjugate with the highest CL signal. The conjugate was isolated through HF5 as previously described and used for the dot-immunobinding assay as detailed in par 2.5. A typical calibration curve was generated as three independent triplicates for Rabbit IgG concentration ranging from 0.08 to 0.5 ng/mL (Supplementary materials, Fig. S3). The low variability obtained from three repeated calibration curves demonstrates good reproducibility of the system. The LOD was estimated as the concentration corresponding to the mean blank value plus three times its standard deviation with a value of 0.26 $\pm$ 0.01pM.

The calculated LOD value is comparable to, or rather slightly lower than, the LODs reported for similar immunoassays employing HRP as the IgG label for CL signal generation (Roda et al., 2020); it is therefore suitable for diagnostic IgG determination (Hettegger et al., 2019).

This outcome is particularly promising considering that a CL substrate optimized for HRP (and not aimed at PtNPs) was used. Further optimization of a substrate specifically tailored for the CL detection of PtNPs could enable these nanozymes to achieve higher sensitivity levels, while offering additional advantages of enhanced robustness and higher stability. In addition the optimal IgG:PtNPs conjugation ratio (from the present pilot study, or for other specific recognition requirements) can be optimized with the HF5 platform, and further isolation of standardized conjugates can be performed following the model study, further elevating the quality and promise of PtNPs nanozyme-based CL probes.

4. Conclusions

The results of the present work demonstrate that HF5 is a fundamental microfluidic tool not only in enabling precise control over the protein-to-nanoparticle conjugation ratio, but also in generating homogeneous nanoparticle-protein probes. Specifically, the HF5 methodology facilitated the rapid screening of optimal conjugation parameters and, more important, the efficient isolation of PtNPs-conjugates with a defined ratio protein:NPs. This rigorous purification strategy enabled the removal of unconjugated species and other interfering components, yielding a highly purified and stable PtNPs-conjugates catalytic system in less than 25 min, providing a more precise and reproducible alternative to conventional centrifugation or chromatographic methods, which frequently fail to yield a clear and pure nanoparticle population. On the other hand, enhanced homogeneity of the PtNPs-conjugates system allows high-performance CL measurements, characterized by strong and stable signals. This great control was paramount in achieving standardized ultrasmall Pt nanoenzymes suitable to be exploited in robust and highly sensitive biosensors. Finally, a pilot study highlights how isolated IgG conjugated-PtNPs can be used in biosensor format for highly sensitive and robust IgG quantification.

Future studies may be directed toward exploring the stability of the conjugates isolated by HF5 under different conditions, depending on the intended application. Distinct experimental conditions could be established according to the specific use of these conjugates, ranging from imaging applications to the fabrication of biosensors for diagnostic and clinical purposes. Moreover, the enhancement of the CL response of these systems could be further supported by the development of specifically designed substrates aimed at improving their catalytic activity.

CRediT authorship contribution statement

Luisa Stella Dolci: Writing – review & editing, Writing – original draft, Validation. **Valentina Marassi:** Writing – review & editing, Data curation. **Stefano Giordani:** Writing – review & editing, Writing – original draft, Validation, Data curation. **Deborah Pedone:** Writing – review & editing, Data curation. **Anna Placci:** Data curation. **Virginia Rondinini:** Data curation. **Erika Scavetta:** Writing – review & editing. **Pierluigi Reschiglian:** Writing – review & editing, Funding acquisition. **Mauro Moglianetti:** Writing – review & editing, Methodology, Conceptualization. **Pier Paolo Pompa:** Writing – review & editing, Methodology. **Andrea Zattoni:** Writing – review & editing, Writing – original draft, Validation. **Barbara Roda:** Writing – review & editing, Writing – original draft, Project administration. **Aldo Roda:** Writing – review & editing, Writing – original draft, Conceptualization.

Declaration of competing interest

The authors declare that they have no known competing financial interests or personal relationships that could have appeared to influence the work reported in this paper.

Acknowledgements

This research was supported by Italian Space Agency (ASI), Project “GRAVI-CUORE: Biosensore multiparametrico per il monitoraggio di marcatori salivari di danno cardiaco in corso di volo umano spaziale”. We also acknowledge the contributions of Valentina Mastronardi and Anna Scarsi for help during PtNP synthesis and characterization. Graphocal Abstract was created in BioRender. Rondinini, V. (2025) https://BioRender.com/l5v53um; Fogure 2 was created in BioRender. Rondinini, V. (2025) https://BioRender.com/49kioro.

Appendix A. Supplementary data

Supplementary data to this article can be found online at https://doi.org/10.1016/j.bios.2025.118295.

Data availability

Data will be made available on request.

References

Bardi, G., Boselli, L., Paolo Pompa, P., 2023. Anti-inflammatory potential of platinum nanozymes: mechanisms and perspectives. Nanoscale 15, 14284–14300. https://doi.org/10.1039/D3NR03016D.

Bhakta, S.A., Evans, E., Benavidez, T.E., Garcia, C.D., 2015. Protein adsorption onto nanomaterials for the development of biosensors and analytical devices: a review. Anal. Chim. Acta 872, 7–25. https://doi.org/10.1016/j.aca.2014.10.031.

Bian, J., Gobalasingham, N., Purchel, A., Lin, J., 2023. The power of field-flow fractionation in characterization of nanoparticles in drug delivery. Molecules 28, 4169. https://doi.org/10.3390/molecules28104169.

Calabria, D., Calabretta, M.M., Zangheri, M., Marchegiani, E., Trozzi, I., Guardigli, M., Michelini, E., Di Nardo, F., Anfossi, L., Baggiani, C., et al., 2021. Recent advancements in enzyme-based lateral flow immunoassays. Sensors 21, 3358. https://doi.org/10.3390/s21103358.

Carvalho, P.M., Felício, M.R., Santos, N.C., Gonçalves, S., Domingues, M.M., 2018. Application of light scattering techniques to nanoparticle characterization and development. Front. Chem. 6. https://doi.org/10.3389/fchem.2018.00237.

Cheng, N., Song, Y., Zeinhom, M.M.A., Chang, Y.-C., Sheng, L., Li, H., Du, D., Li, L., Zhu, M.-J., Luo, Y., et al., 2017. Nanozyme-mediated dual immunoassay integrated with smartphone for use in simultaneous detection of pathogens. ACS Appl. Mater. Interfaces 9, 40671–40680. https://doi.org/10.1021/acsami.7b12734.

Choi, G., Kim, E., Park, E., Lee, J.H., 2017. A cost-effective chemiluminescent biosensor capable of early diagnosing cancer using a combination of magnetic beads and platinum nanoparticles. Talanta 162, 38–45. https://doi.org/10.1016/j.talanta.2016.09.061.

Contado, C., 2017. Field flow fractionation techniques to explore the “Nano-World.”. Anal. Bioanal. Chem. 409, 2501–2518. https://doi.org/10.1007/s00216-017-0180-6.

Cupini, S., Di Marco, S., Boselli, L., Cavalli, A., Tarricone, G., Mastronardi, V., Castagnola, V., Colombo, E., Pompa, P.P., Benfenati, F., 2023. Platinum nanozymes counteract photoreceptor degeneration and retina inflammation in a light-damage model of age-related macular degeneration. ACS Nano 17, 22800–22820. https://doi.org/10.1021/acsnano.3c07517.

Cursi, L., Mirra, G., Boselli, L., Pompa, P.P., 2024. Metrology of platinum nanozymes: mechanistic insights and analytical issues. Adv. Funct. Mater. 34, 2315587. https://doi.org/10.1002/adfm.202315587.

De Luca, E., Pedone, D., Scarsi, A., Marotta, R., Catalano, F., Debellis, D., Cursi, L., Grimaldi, B., Moglianetti, M., Pompa, P.P., 2024. Platinum nanozyme probes for cellular imaging by electron microscopy. Small Sci. 4, 2400085. https://doi.org/10.1002/smsc.202400085.

DNA-based platinum nanozymes for peroxidase mimetics | J. Phys. Chem. C Available online: https://pubs.acs.org/doi/full/10.1021/jp503242e (accessed on 14 November 2025).

Dubascoux, S., Von Der Kammer, F., Le Hécho, I., Gautier, M.P., Lespes, G., 2008. Optimisation of asymmetrical flow field flow fractionation for environmental nanoparticles separation. J. Chromatogr. A 1206, 160–165. https://doi.org/10.1016/j.chroma.2008.07.032.

Ferreira, H.S., Moreira-Alvarez, B., Montoro Bustos, A.R., Encinar, J.R., Costa-Fernández, J.M., Sanz-Medel, A., 2020. Capabilities of asymmetrical flow field – flow fractionation on-Line coupled to different detectors for characterization of water-stabilized quantum dots bioconjugated to biomolecules. Talanta 206, 120228. https://doi.org/10.1016/j.talanta.2019.120228.

Gao, Z., Ye, H., Tang, D., Tao, J., Habibi, S., Minerick, A., Tang, D., Xia, X., 2017. Platinum-decorated gold nanoparticles with dual functionalities for ultrasensitive colorimetric in vitro diagnostics. Nano Lett. 17, 5572–5579. https://doi.org/10.1021/acs.nanolett.7b02385.

Gatto, F., Cagliani, R., Catelani, T., Guarnieri, D., Moglianetti, M., Pompa, P.P., Bardi, G., 2017. PMA-induced THP-1 macrophage differentiation is not impaired by citrate-coated platinum nanoparticles. Nanomaterials 7, 332. https://doi.org/10.3390/nano7100332.

Giordani, S., Marassi, V., Placci, A., Zattoni, A., Roda, B., Reschiglian, P., 2023. Field-flow fractionation in molecular biology and biotechnology. Molecules 28, 6201. https://doi.org/10.3390/molecules28176201.

Gold-platinum nanoflowers as a label and as an enzyme mimic for use in highly sensitive lateral flow immunoassays: application to detection of rabbit IgG | Microchim. Acta Available online: https://link.springer.com/article/10.1007/s00604-019-3464-z (accessed on 14 November 2025).

Hamed, E.M., Fung, F.M., Li, S.F.Y., 2025. Nanozymes and the sustainable future of food quality control: innovation versus pragmatism. ACS Food Sci. Technol. 5, 925–927. https://doi.org/10.1021/acsfoodscitech.4c01040.

Hettegger, P., Huber, J., Paßecker, K., Soldo, R., Kegler, U., Nöhammer, C., Weinhäusel, A., 2019. High similarity of IgG antibody profiles in blood and saliva opens opportunities for saliva based serology. PLoS One 14, e0218456. https://doi.org/10.1371/journal.pone.0218456.

Hornberger, E., Mastronardi, V., Brescia, R., Pompa, P.P., Klingenhof, M., Dionigi, F., Moglianetti, M., Strasser, P., 2021. Seed-mediated synthesis and catalytic ORR reactivity of facet-stable, monodisperse platinum nano-octahedra. ACS Appl. Energy Mater. 4, 9542–9552. https://doi.org/10.1021/acsaem.1c01696.

Il Kim, M., Su Kim, M., Woo, M.-A., Ye, Y., Suk Kang, K., Lee, J., Gyu Park, H., 2014. Highly efficient colorimetric detection of target cancer cells utilizing superior catalytic activity of graphene Oxide–magnetic-platinum nanohybrids. Nanoscale 6, 1529–1536. https://doi.org/10.1039/C3NR05539F.

Jiang, T., Song, Y., Wei, T., Li, H., Du, D., Zhu, M.-J., Lin, Y., 2016. Sensitive detection of *Escherichia coli* O157:H7 using Pt–Au bimetal nanoparticles with peroxidase-like amplification. Biosens. Bioelectron. 77, 687–694. https://doi.org/10.1016/j.bios.2015.10.017.

Lespes, G., De Carsalade Du Pont, V., 2022. Field-flow fractionation for nanoparticle characterization. J. Sep. Sci. 45, 347–368. https://doi.org/10.1002/jssc.202100595.

Li, W., Chen, B., Zhang, H., Sun, Y., Wang, J., Zhang, J., Fu, Y., 2015. BSA-stabilized Pt nanozyme for peroxidase mimetics and its application on colorimetric detection of Mercury(II) ions. Biosens. Bioelectron. 66, 251–258. https://doi.org/10.1016/j.bios.2014.11.032.

Liu, S., Dou, L., Yao, X., Zhang, W., Zhao, M., Yin, X., Sun, J., Zhang, D., Wang, J., 2020. Nanozyme amplification mediated On-Demand multiplex lateral flow immunoassay with dual-readout and broadened detection range. Biosens. Bioelectron. 169, 112610. https://doi.org/10.1016/j.bios.2020.112610.

López-Sanz, S., Fariñas, N.R., Martín-Doimeadios, R., del, C.R., Ríos, Á., 2019. Analytical strategy based on asymmetric flow field flow fractionation hyphenated to ICP-MS and complementary techniques to study gold nanoparticles transformations in cell culture medium. Anal. Chim. Acta 1053, 178–185. https://doi.org/10.1016/j.aca.2018.11.053.

Loynachan, C.N., Thomas, M.R., Gray, E.R., Richards, D.A., Kim, J., Miller, B.S., Brookes, J.C., Agarwal, S., Chudasama, V., McKendry, R.A., et al., 2018. Platinum nanocatalyst amplification: redefining The Gold standard for lateral flow immunoassays with ultrabroad dynamic range. ACS Nano 12, 279–288. https://doi.org/10.1021/acsnano.7b06229.

Marassi, V., Beretti, F., Roda, B., Alessandrini, A., Facci, P., Maraldi, T., Zattoni, A., Reschiglian, P., Portolani, M., 2019. A new approach for the separation, characterization and testing of potential prionoid protein aggregates through hollow-fiber flow field-flow fractionation and multi-angle light scattering. Anal. Chim. Acta 1087, 121–130. https://doi.org/10.1016/j.aca.2019.08.003.

Marassi, V., Giordani, S., Placci, A., Punzo, A., Caliceti, C., Zattoni, A., Reschiglian, P., Roda, B., Roda, A., 2023. Emerging microfluidic tools for simultaneous exosomes and cargo biosensing in liquid biopsy: new integrated miniaturized FFF-assisted approach for Colon cancer diagnosis. Sensors 23, 9432. https://doi.org/10.3390/s23239432.

Marassi, V., Wang, J., Giordani, S., Placci, A., Roda, B., Reschiglian, P., Zattoni, A., 2025. A direct, real-time, size-resolved analytical strategy to follow drug loading and release from biocompatible gold nanoparticles. Anal. Chim. Acta 1365, 344246. https://doi.org/10.1016/j.aca.2025.344246.

Mastronardi, V., Udayan, G., Cibecchini, G., Brescia, R., Fichthorn, K.A., Pompa, P.P., Moglianetti, M., 2020. Synthesis of citrate-coated penta-twinned palladium nanorods and ultrathin nanowires with a tunable aspect ratio. ACS Appl. Mater. Interfaces 12, 49935–49944. https://doi.org/10.1021/acsami.0c11597.

Mastronardi, V., Magliocca, E., Gullon, J.S., Brescia, R., Pompa, P.P., Miller, T.S., Moglianetti, M. Ultrasmall, 2022. Coating-free, pyramidal platinum nanoparticles for high stability fuel cell oxygen reduction. ACS Appl. Mater. Interfaces 14, 36570–36581. https://doi.org/10.1021/acsami.2c07738.

Mazzotta, E., Di Giulio, T., Mastronardi, V., Brescia, R., Pompa, P.P., Moglianetti, M., Malitesta, C., 2023. Nanozymes Based on Octahedral Platinum Nanocrystals with {111} Surface Facets: Glucose Oxidase Mimicking Activity in Electrochemical Sensors. Microchim. Acta 190, 425. https://doi.org/10.1007/s00604-023-05992-9.

Mirra, G., Cursi, L., Boselli, L., Pompa, P.P., 2025. Screening oxidoreductase activities of nanozymes: toward activity-tailored guidelines. Small Sci. 5, 2400487. https://doi.org/10.1002/smsc.202400487.

Nelli, D., Mastronardi, V., Brescia, R., Pompa, P.P., Moglianetti, M., Ferrando, R., 2023. Hydrogen promotes the growth of platinum pyramidal nanocrystals by size-dependent symmetry breaking. Nano Lett. 23, 2644–2650. https://doi.org/10.1021/acs.nanolett.2c04982.

Park, J.-M., Jung, H.-W., Chang, Y.W., Kim, H.-S., Kang, M.-J., Pyun, J.-C., 2015. Chemiluminescence lateral flow immunoassay based on Pt nanoparticle with peroxidase activity. Anal. Chim. Acta 853, 360–367. https://doi.org/10.1016/j.aca.2014.10.011.

Pedone, D., Moglianetti, M., Luca, E.D., Bardi, G., Paolo Pompa, P., 2017. Platinum nanoparticles in nanobiomedicine. Chem. Soc. Rev. 46, 4951–4975. https://doi.org/10.1039/C7CS00152E.

Pedone, D., Moglianetti, M., Lettieri, M., Marrazza, G., Pompa, P.P., 2020. Platinum nanozyme-enabled colorimetric determination of total antioxidant level in saliva. Anal. Chem. 92, 8660–8664. https://doi.org/10.1021/acs.analchem.0c01824.

Ramm, I., Leeman, M., Schagerlöf, H., León, I.R., Castro, A., Nilsson, L., 2022. Investigation of native and aggregated therapeutic proteins in human plasma with asymmetrical flow field-flow fractionation and mass spectrometry. Anal. Bioanal. Chem. 414, 8191–8200. https://doi.org/10.1007/s00216-022-04355-2.

Reyes, S., Rizzo, E., Ting, A., Dikici, E., Daunert, S., K. Deo, S., 2022. Metal organic framework encapsulated Tamavidin-Gluc reporter: application in COVID-19 spike antigen bioluminescent immunoassay. Sens. Diagn. 1, 1198–1208. https://doi.org/10.1039/D2SD00145D.

Roda, A., Arduini, F., Mirasoli, M., Zangheri, M., Fabiani, L., Colozza, N., Marchegiani, E., Simoni, P., Moscone, D., 2020. A challenge in biosensors: is it better to measure a photon or an electron for ultrasensitive detection? Biosens. Bioelectron. 155, 112093. https://doi.org/10.1016/j.bios.2020.112093.

Roda, B., Deo, S.K., O'Connor, G., Moraskie, M., Giordani, S., Marassi, V., Roda, A., Daunert, S., 2024. Shining light on biosensors: chemiluminescence and bioluminescence in enabling technologies. TrAC Trends Anal. Chem. 180, 117975. https://doi.org/10.1016/j.trac.2024.117975.

Ruditskiy, A., Xia, Y., 2017. The science and art of carving metal nanocrystals. ACS Nano 11, 23–27. https://doi.org/10.1021/acsnano.6b08556.

Sánchez-Cachero, A., López-Sanz, S., Fariñas, N.R., Ríos, Á., Martín-Doimeadios, R., del, C.R., 2021. A method based on asymmetric flow field flow fractionation hyphenated to inductively coupled plasma mass spectrometry for the monitoring of platinum nanoparticles in water samples. Talanta 222, 121513. https://doi.org/10.1016/j.talanta.2020.121513.

Scarsi, A., Pedone, D., Paolo Pompa, P., 2023. A multi-line platinum nanozyme-based lateral flow device for the colorimetric evaluation of total antioxidant capacity in different matrices. Nanoscale Adv. 5, 2167–2174. https://doi.org/10.1039/D2NA00931E.

Sitar, S., Vezočnik, V., Maček, P., Kogej, K., Pahovnik, D., Žagar, E., 2017. Pitfalls in size characterization of soft particles by dynamic light scattering online coupled to asymmetrical flow field-flow fractionation. Anal. Chem. 89, 11744–11752. https://doi.org/10.1021/acs.analchem.7b03251.

Soliman, M.G., Martinez-Serra, A., Dobricic, M., Trinh, D.N., Cheeseman, J., Spencer, D.I. R., Monopoli, M.P., 2024. Protocols for isolation and characterization of nanoparticle biomolecular Corona complexes. Front. Toxicol. 6. https://doi.org/10.3389/ftox.2024.1393330.

Su, H., Zhao, H., Qiao, F., Chen, L., Duan, R., Ai, S., 2013. Colorimetric detection of Escherichia coli O157:H7 using functionalized Au@Pt nanoparticles as peroxidase mimetics. Analyst 138, 3026–3031. https://doi.org/10.1039/C3AN00026E.

Tan, Z.-Q., Liu, J.-F., Guo, X.-R., Yin, Y.-G., Byeon, S.K., Moon, M.H., Jiang, G.-B., 2015. Toward full spectrum speciation of silver nanoparticles and ionic silver by On-Line coupling of hollow fiber flow field-flow fractionation and minicolumn concentration with multiple detectors. Anal. Chem. 87, 8441–8447. https://doi.org/10.1021/acs.analchem.5b01827.

Tan, Z.-Q., Yin, Y.-G., Guo, X.-R., Amde, M., Moon, M.H., Liu, J.-F., Jiang, G.-B., 2017. Tracking the transformation of nanoparticulate and ionic silver at environmentally relevant concentration levels by hollow fiber flow field-flow fractionation coupled to ICPMS. Environ. Sci. Technol. 51, 12369–12376. https://doi.org/10.1021/acs.est.7b03439.

Tarricone, G., Castagnola, V., Mastronardi, V., Cursi, L., Debellis, D., Ciobanu, D.Z., Armirotti, A., Benfenati, F., Boselli, L., Pompa, P.P., 2023. Catalytic bioswitch of platinum nanozymes: mechanistic insights of reactive oxygen species scavenging in

the neurovascular unit. Nano Lett. 23, 4660–4668. https://doi.org/10.1021/acs.nanolett.3c01479.

Tseng, C.-W., Chang, H.-Y., Chang, J.-Y., Huang, C.-C., 2012. Detection of mercury ions based on mercury-induced switching of enzyme-like activity of platinum/gold nanoparticles. Nanoscale 4, 6823–6830. https://doi.org/10.1039/C2NR31716H.

Wang, Z., Yao, X., Zhang, Y., Wang, R., Ji, Y., Sun, J., Zhang, D., Wang, J., 2020a. Functional nanozyme mediated multi-readout and label-free lateral flow immunoassay for rapid detection of *Escherichia Coli* O157:H7. Food Chem. 329, 127224. https://doi.org/10.1016/j.foodchem.2020.127224.

Wang, Z., Dong, B., Cui, X., Fan, Q., Huan, Y., Shan, H., Feng, G., Fei, Q., 2020b. Core-shell Au@Pt nanoparticles catalyzed luminol chemiluminescence for sensitive detection of thiocyanate. Anal. Sci. 36, 1045–1051. https://doi.org/10.2116/analsci.19P475.

Wang, Z., Hu, J., Wang, H., 2024. Hierarchical polyimide microparticles with controllable morphology. Small 20, 2400487. https://doi.org/10.1002/smll.202400487.

Wei, H., Wang, E., 2013. Nanomaterials with enzyme-like characteristics (Nanozymes): next-generation artificial enzymes. Chem. Soc. Rev. 42, 6060–6093. https://doi.org/10.1039/C3CS35486E.

Wei, D., Zhang, X., Chen, B., Zeng, K., 2020. Using bimetallic Au@Pt nanozymes as a visual tag and as an enzyme mimic in enhanced sensitive lateral-flow immunoassays: application for the detection of streptomycin. Anal. Chim. Acta 1126, 106–113. https://doi.org/10.1016/j.aca.2020.06.009.

Xu, S.-L., Cui, H., 2007. Luminol chemiluminescence catalysed by colloidal platinum nanoparticles. Luminescence 22, 77–87. https://doi.org/10.1002/bio.929.

Xu, J., Zhao, S., Zhang, Q., Huang, X., Du, K., Wang, J., Wang, J., Chen, C., Zhang, B., Chang, J., et al., 2024. Development of highly sensitive dual-enhanced fluorescence quenching immunochromatographic test strips based on Pt nanoprobes. Biosens. Bioelectron. 254, 116195. https://doi.org/10.1016/j.bios.2024.116195.

Yang, X., Porcel, E., Marichal, L., Gonzalez-Vargas, C., Khitous, A., Salado-Leza, D., Li, X., Renault, J.-P., Pin, S., Remita, H., et al., 2024. Human serum albumin in the presence of small platinum nanoparticles. J. Pharm. Sci. 113, 1645–1652. https://doi.org/10.1016/j.xphs.2024.02.002.

Zappi, A., Marassi, V., Kassouf, N., Giordani, S., Pasqualucci, G., Garbini, D., Roda, B., Zattoni, A., Reschiglian, P., Melucci, D., 2022. A green analytical method combined with chemometrics for traceability of tomato sauce based on colloidal and volatile fingerprinting. Molecules 27, 5507. https://doi.org/10.3390/molecules27175507.

Zhang, Y., Zhao, Q., Zhang, M., Na, N., Ouyang, J., Shen, X., 2025a. Recent progress in the rational design and applications of nanozymes. Biomed. Anal. 2, 25–38. https://doi.org/10.1016/j.bioana.2025.02.001.

Zhang, W., Shu, J., Wang, M., Zheng, K., Cui, H., 2025b. One-pot synthesis of N-(4-Aminobutyl)-N-Ethylisoluminol doping cuprous oxide nanocubes for label-free chemiluminescence immunoassay of cardiac troponin I. Anal. Chem. 97, 12116–12124. https://doi.org/10.1021/acs.analchem.5c00462.